Heliyon

ELSEVIER

Received:
8 November 2016
Revised:
26 December 2016
Accepted:
30 January 2017

Heliyon 3 (2017) e00241

Saharan dust detection using multi-sensor satellite measurements

Sriharsha Madhavan [a,b,c,*], **John J. Qu** [a], **X. Hao** [a]

[a] *Environmental Science and Technology Center, Department of Geography and Geoinformation Sciences, George Mason University, 4400 University Drive, Fairfax, VA 22030, USA*

[b] *NOAA National Environmental Satellite, Data, and Information Service Center for Satellite Applications and Research, E/RA3, 5830 University Research Ct., College Park, MD 20740, USA*

[c] *Science Systems and Applications Inc., 10210 Greenbelt Rd., Lanham, MD 20706, USA*

* Corresponding author.

E-mail address: sriharsha.madhavan@ssaihq.com (S. Madhavan).

Abstract

Contemporary scientists have vested interest in trying to understand the climatology of the North Atlantic Basin since this region is considered as the genesis for hurricane formation that eventually get shipped to the tropical Atlantic region and the Caribbean. The effects of atmospheric water cycle and the climate of West Africa and the Atlantic basin are hugely impacted by the radiative forcing of Saharan dust. The focus area in this paper would be to improve the dust detection schemes by employing the use of multi sensor measurements in the thermal emissive wavelengths using legacy sensors such as Terra (T) and Aqua (A) MODerate-resolution Imaging Spectroradiometer (MODIS), fusing with Ozone Monitoring Instrument (OMI). Previous work by Hao and Qu (2007) had considered a limited number of thermal infrared channels which led to a correlation coefficient R^2 value of 0.765 between the Aerosol Optical Thickness (AOT) at 550 nm and the modeled dust index. In this work, we extend the thermal infrared based dust detection by employing additional channels: the 8.55 μm which has shown high sensitivity to the Saharan dust, along with water vapor channel of 7.1 μm and cloud top channel of 13.1 μm. Also, the dust pixels were clearly identified using the OMI based aerosol types. The dust pixels were cleanly segregated from the other aerosol types such as sulfates, biomass, and other carbonaceous aerosols.

http://dx.doi.org/10.1016/j.heliyon.2017.e00241

These improvements led to a much higher correlation coefficient R^2 value of 0.85 between the modified dust index and the AOT in comparison to the previous work. The key limitations from the current AOT products based on MODIS and were put to test by validating the improved dust detection algorithm. Two improvements were noted. First, the dust measurement radiometry using MODIS is significantly improved by at least an order of 2. Second the spatial measurements are enhanced by a factor of at least 10.

Keywords: Atmospheric science, Environmental science, Geography, Geology, Geophysics

1. Introduction

Dust monitoring is one of the most perplexing issues in today's aerosol remote sensing. Some of the major obstacles are compounded in nature. Even though the Earth observing instruments, such as MODerate Resolution Imaging Spectro-radiometer (MODIS), are versatile instruments for measurement of aerosols, the problem in identifying dust aerosol is huge; and is mainly due to the inability to distinguish dust features from similar spectrally looking components in the atmosphere. Since the desert is a bright surface in the visible channels, it poses another issue of distinguishing (or in other words decoupling) surface reflectivity and atmospheric contributions. Most of the current approaches deal with modeling the atmosphere through radiative transfer equations that best simulate the observing conditions (Holben et al., 2001; Kaufman et al., 1997; Tanré et al., 1997; Mishchenko et al., 1999; Hsu et al., 2004; Remer et al., 2005; Grey et al., 2006). Such an approach would work well, so long as the atmospheric components do not vary significantly. In the case of dust aerosols this is a precarious assumption. A physical theoretical algorithm is devised in this paper that tries to address areas where dust monitoring could be improved.

Previous work as reported by Hao and Qu (2007) established a relationship between the Aerosol Optical Thickness (AOT) as measured in the 0.550 μm and the MODIS thermal channels Bands 20, 30, 31 and 32. Based on the sensitivity analysis the authors found the dust to be widely varying in the 11 μm and 12 μm channels, respectively. A difference of the brightness temperatures between Bands 32 and 31 seem to show a clear distinction between heavy aerosol loading due to dust vs. low aerosol concentration. Also, MODIS bands 20 and 30 have a high level of sensitivity to dust. However, the sensitivity also leads to large standard deviation thereby diminishing the accuracy of establishing a good relationship between aerosol loading and the brightness temperature differences between Band 20 and 30. Therefore in order to distinguish between heavy dust and low aerosol concentrations the authors come up with an empirical equation (refer (1)) that relates the measured AOT in 0.550 μm to the MODIS bands 20, 30, 31, and 32.

http://dx.doi.org/10.1016/j.heliyon.2017.e00241

$$AOT(550\ nm) = c0 + c1*BT20 + c2*BT30 + c3*BT31 + c4*BT32 \quad (1)$$

The validation of the above approach has shown very promising results. A one-to-one comparison of the thermal dust index and the retrieved AOT using the MODIS Level 2 product seem to have a good correlation ($R^2 = 0.765$). In this work, we extend the previous success of the thermal infrared based dust detection by using wavelengths that show more sensitivity to the Saharan dust. As a result, the dust radiometry would be further enhanced leading to greater accuracy in measuring the dust intensity over the North Atlantic basin.

The paper is broken down as follows. First, an approach is developed which in many ways are to address the limitations of the traditionally used metric of AOT to quantify the large dust particles. The improvement in dust monitoring is exploited using MODIS band 29 which is mostly used in cloud detection. The background for this is given in Section 2. The characterization and the formulation for dust detection are described in the Section 3. This is followed by the qualitative and quantitative validation and is presented in Section 4. Finally, the paper is closed with a complete synopsis of the work using the presented results.

2. Background

In this section, we focus on the improvement in dust detection by mitigating the use of the 8.55 μm channel (band 29).

First, we try to understand the importance of the 8.55 μm channel in dust detection. For most dust classification, ice and water clouds are the chief distorting features as they are not easily distinguishable from dust clouds. Hence a careful understanding of the spectral sensitivity Saharan dust and the other major contributing features such as water, ice are imperative. Since we are in the thermal infrared wavelengths a key geophysical quantity the emissivity spectral curve becomes very vital; also, an *a priori* knowledge of the major contributing mineral composition of the Saharan dust. Menéndez et al. (2007) in their report had identified 'Quartz' in varied forms to be the dominant mineral element (> 46%) of the coarser elements i.e. particle size greater than 75 μm. Similar findings have been reported historically by Wald (1995). The next step is to identify closely the spectral sensitivity of the Quartz mineral of particle size ≥ 75 μm. The Arizona State University (ASU) spectral library (Christensen et al., 2000) houses hundreds of mineral spectral signatures. We tease out the emissivity curves for the two dominant features 1. Quartz mineral of particle size ≥ 75 μm and 2. (ice, water) in the Long Wave InfraRed (LWIR) wavelengths.

A couple of interesting spectral behavior is noted for the aforementioned two types of features under study. The emissivity curves for this study are shown in Fig. 1. Based on Fig. 1, the following are deduced. First, the Quartz mineral has an

http://dx.doi.org/10.1016/j.heliyon.2017.e00241

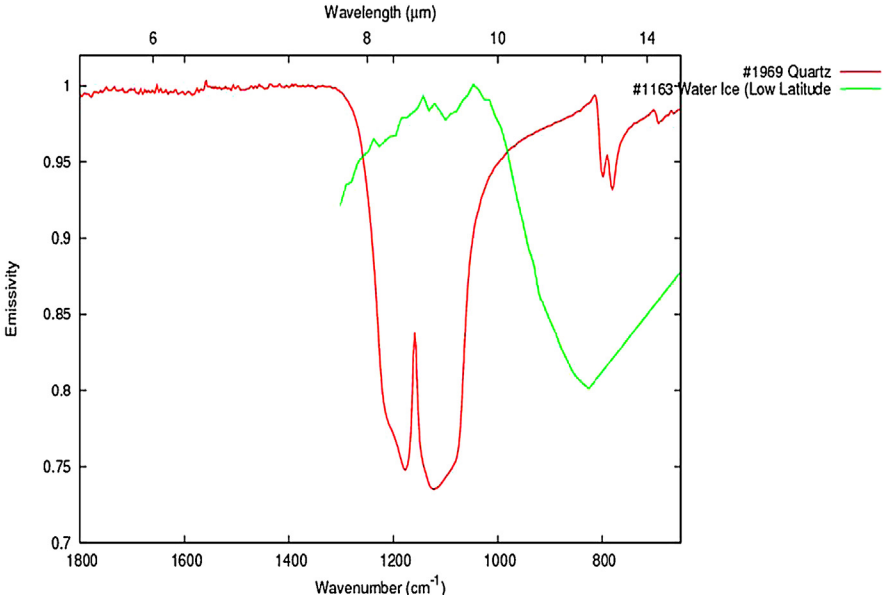

Fig. 1. Emissivity curves for a. Quartz (red line), b. ice, water (green line) (ASU spectral library: http://speclib.asu.edu/).

emissivity curve close to 0.98 from around 5.5 μm up until the 8 μm wavelength, from there on until 8.5 there is a drop in the emissivity to about 0.75 and a distinct peak up to 0.83 is observed at approximately 8.55 μm. The curve then takes another dip and reaches about 0.74 close to the 9 μm wavelength. From there on a rapid increase in the emissivity to about 0.97 is observed up to the 11 μm. This difference in emissivity is very unique to a mineral like Quartz and can be exploited for the dust detection by choosing the 8.55 μm and 11 μm wavelengths. In contrast, features like ice and water seem to be on the flip at the two wavelengths mentioned above. From the curve, it is noted that these features have a higher emissivity of approximately 0.97 at 8.55 μm and a low emissivity of approximately 0.8 at 11 μm. Also, it is noted that the emissivity curves for ice and water are shown for lower latitudes, very similar curve is obtained at higher latitudes, is not shown here for convenience. This dichotomy of the emissivity will be further exploited in the dust detection.

3. Methodology

Previous work by Hao and Qu (2007), demonstrated the sensitivity of the thermal infrared channels to dust and found certain combinations to be highly useful in differentiating dust from other aerosols and cloud. In this section, a lead from the previous work is extended by employing a higher correlation set of Mid Wave InfraRed (MWIR) and LWIR spectral responses to the AOT. One of the neat advantages of using the far Infrared channels is the night time detection along with the day time dust outbreaks. This is a disadvantage with the previous approach. In

http://dx.doi.org/10.1016/j.heliyon.2017.e00241

general, the dust aerosols were highly correlated in the Brightness Temperature (BT) space. In other words, the BT difference between 3.7 μm and 12 μm and BT difference between 11 μm and 12 μm were highly correlated to the dust thickness (Ackerman, 1997). In addition, in this work, the water vapor channels 7.1 μm, the dust sensitive channel 8.5 μm, and the cloud top channel of 13.1 μm are combined. In terms of MODIS the channels used correspond to bands 20, 28, 29, 31, 32 and

Table 1. List of MODIS granules for dust storm detection scheme.

No.	Granule id Julian day, UTC T-MODIS	Granule id Julian day, UTC A-MODIS
1	2000057.1140	2002195.1455
2	2000060.1215	2003156.1415
3	2002007.1125	2005008.1415
4	2002181.1140	2005008.1420
5	2003155.1205	2005043.1450
6	2003155.1210	2005046.1345
7	2005007.1210	2005136.1420
8	2005043.1145	2005139.1450
9	2005136.1115	2005200.1420
10	2005136.1120	2005227.1405
11	2005136.1255	2005247.1515
12	2005139.1145	2006067.1335
13	2005139.1150	2006067.1510
14	2005200.1115	2007003.1440
15	2005227.1055	2007060.1435
16	2005247.1210	2007129.1455
17	2006067.1205	2008089.1510
18	2007003.1135	2009155.1515
19	2007003.1140	2009173.1505
20	2007060.1130	2010206.1515
21	2007129.1150	2010259.1355
22	2008089.1205	2010259.1530
23	2008089.1210	2011196.1405
24	2009155.1210	2011266.1505
25	2009173.1155	2012079.1455
26	2010206.1205	2012233.1355
27	2010259.1225	
28	2011136.1215	
29	2011196.1055	
30	2011266.1200	

http://dx.doi.org/10.1016/j.heliyon.2017.e00241

33. The datasets used in the characterization are summarized in Table 1. The Saharan dust datasets were identified based on the previous time series analysis work (Madhavan et al., 2016), which comprised of region with geographical co-ordinates (-44.12° W, 36.42° N, 5.02° S, 15.72° E).

In this study, a database comprising of dust laden scenes (identified in Table 1) of MODIS BT and AOT data at 10 km resolution is built. The competence of dust storm detection with MODIS Thermal channels as highlighted is investigated through statistical analysis, and a spectral index, namely Thermal Emissive Dust Index (TEDI), is designed.

Based on the datasets shown in Table 1, the TEDI built using the MWIR and LWIR channels are modeled as a multiple regression with the AOT (refer equation (2)). Table 2 and Table 3 give the multiple regression model and the corresponding coefficients and standard errors of the fitted model for both T- and A- MODIS measurements.

$$TEDI = C0 + C1*BT20 + C2*BT28 + C3*BT29 + C4*BT31 + C5*BT32 + C6*BT33 \quad (2)$$

Since both MODIS instruments are very similar in design, the measurements and the derived TEDI regression coefficients are quite akin. Fig. 2 shows the correlation plot of the modeled TEDI and the AOT. Also, provided are the R^2 coefficients for the same. The R^2 values for both MODIS measurements are 0.81. In the next section a detailed discussion covering the qualitative and quantitative assessment of the TEDI is provided, further improvement of the TEDI by fusing the OMI datasets is also discussed.

4. Results and discussion

This section is primarily broken into two subparts. The first subpart provides a detailed qualitative and quantitative assessment of the TEDI. Next, the section provides an improvement of the TEDI for A-MODIS by synergistically using the Ozone Monitoring Instrument (OMI) aerosol information.

In the case of T-MODIS the granule id shown in no. 8 of Table 1 is chosen for the validation, granule id shown in no. 5 of Table 1 is chosen for A-MODIS. Fig. 3a. shows the MODIS RGB image that clearly identifies the Saharan dust transport

Table 2. Regression model coefficients and standard errors for T-MODIS.

Constant:	-8.80671					
Coefficients:	0.095194	-0.01647	0.199067	-0.81164	0.549136	0.016876
Standard errors:	0.000338	0.000298	0.00208	0.002438	0.00168	0.000661

http://dx.doi.org/10.1016/j.heliyon.2017.e00241

Table 3. Regression model coefficients and standard errors for A-MODIS.

Constant:	-14.0559					
Coefficients:	0.103137	-0.01307	0.161798	-0.5999	0.390936	0.006144
Standard errors:	0.000346	0.000323	0.002629	0.00277	0.001895	0.000736

over the North Atlantic. On the top right, Fig. 3b shows the AOT retrieval, Fig. 3c shows the TEDI retrieval based on the characterization discussed above. As highlighted, the TEDI is provided at a much higher spatial resolution in comparison to the 10 km x 10 km spatially aggregated AOT retrieval. This coupled with the finer radiometric resolution of the identified dust intensity can be seen from Fig. 3c. Further, quantification using the histogram charts is provided by Fig. 4.

From Fig. 4, it is evident from the various peaks and valleys of the histogram, that the pixel level classification of various features is indeed quite good. Quantitatively, the peak at value close to 0.5 identifies the ocean surface; a bell-shaped curve from about 2 onwards represents the dust features, various smaller peaks at roughly 2.5 or so gives the intensified dust pixels. Based on the qualitative assessment the TEDI image indeed, consistent with T-MODIS outscores the AOT retrieval in monitoring the dust pixels. Even though the TEDI does a very good job of identifying the dust pixels, there does seem slight coarseness in terms of the dust radiometry. It is clear that different aerosol types are not segregated completely. This is understood from the scatter charts shown in Fig. 2a and b, these are the smoke, dust and sulfate aerosols respectively. Thus, an additional step is undertaken in order to improve the TEDI model. In order to achieve this, satellite measurements of the Ozone Monitoring Instrument (OMI) is used to identify the various aerosol types as listed above. The OMI sensor is contribution to the Aura Platform which is part of the A-train of platforms that contributes measurements

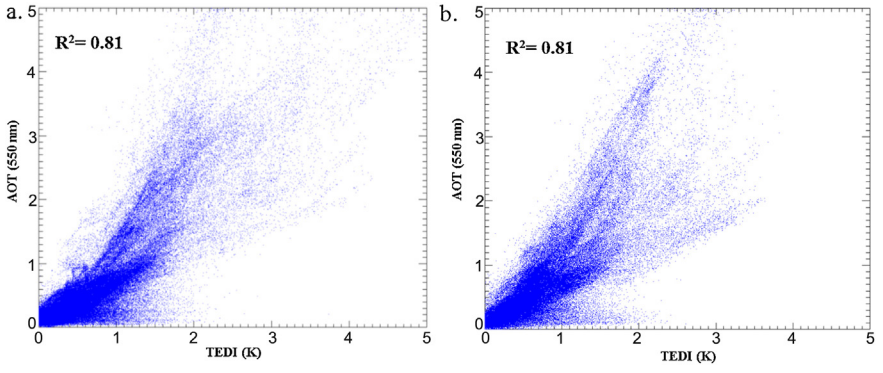

Fig. 2. Scatter plot of AOT and TEDI: a. T-MODIS measurements, b. A-MODIS measurements.

http://dx.doi.org/10.1016/j.heliyon.2017.e00241

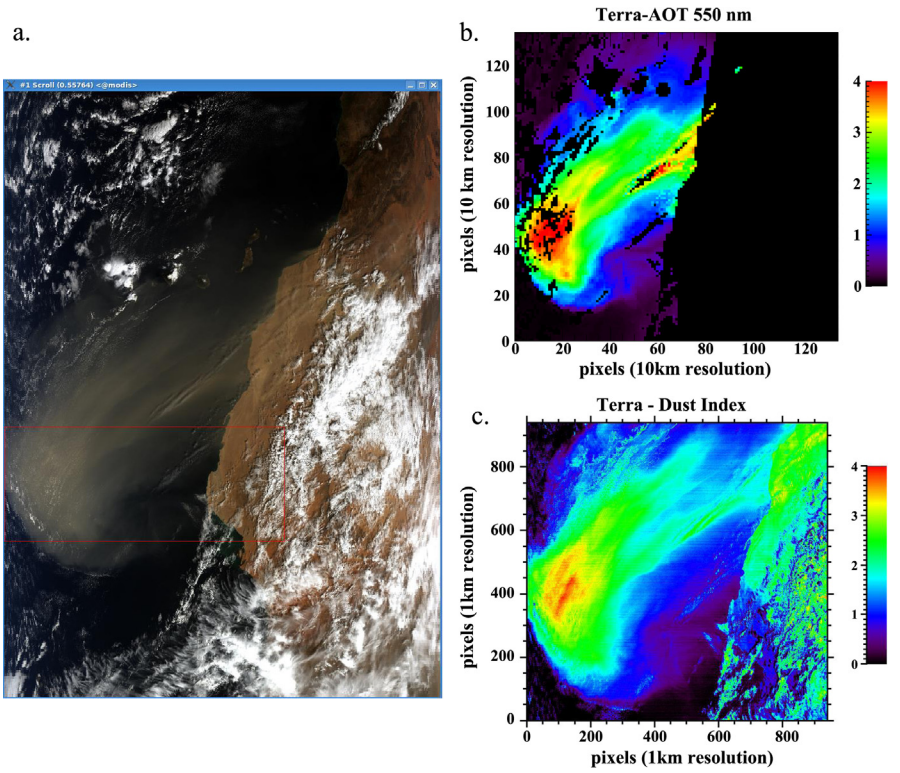

Fig. 3. Validation Scene T-MODIS: a. RGB, b. AOT retrieval, c. TEDI retrieval.

taken by other Earth based remote sensors including the Aqua platform (Levelt et al., 2006). The idea of using the Aura (OMI) and the A-MODIS is to synergistically fuse the two data sets and differentiate the dust aerosols from the

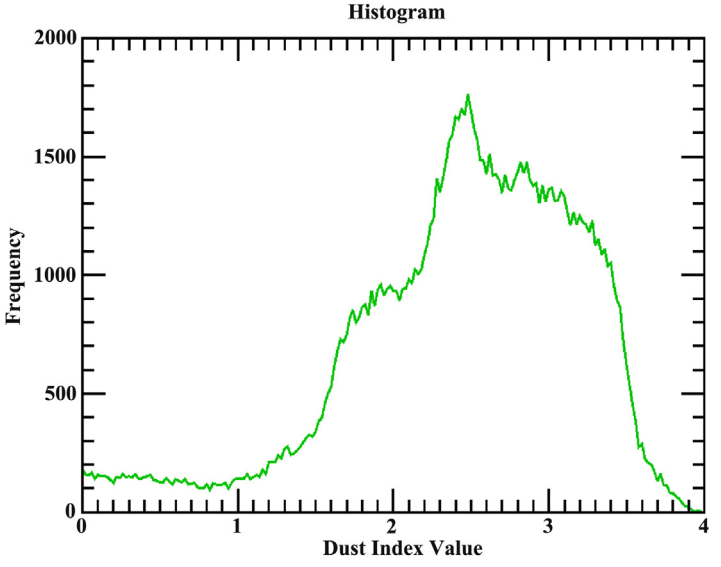

Fig. 4. Quantitative Validation: Histogram of TEDI retrieval.

http://dx.doi.org/10.1016/j.heliyon.2017.e00241

Table 4. Regression model coefficients and standard errors for TEDI using Aura OMI and A-MODIS.

Constant:	-18.7277					
Coefficients:	0.143230	0.004944	-0.090525	-0.293436	0.235151	0.069920
Standard errors:	0.001428	0.001209	0.011332	0.010951	0.008038	0.003069

rest. This requires a good spatial match up of the pixels. Since both instruments are on the same orbit, with a time difference between the two sensor measurements being approximately 10 minutes, a very reasonable assumption is made: the dust transport is invariant over the Ocean surface. The OMI datasets were obtained from the NASA Goddard Earth Sciences Data and Information Services Center (http://disc.sci.gsfc.nasa.gov/Aura/data-holdings/OMI/omaeruv_v003.shtml).

Based on the above-mentioned details, datasets shown in Table 1 between A-MODIS dust granules were matched up with the Aura OMI datasets. Once the dust pixels are collected, the TEDI characterization is re done with these newly classified pixels from the OMI aerosol type. Table 4 gives the TEDI multiple regression model similar to the ones shown in Table 3.

Fig. 5 shows a scatter plot of AOT at 550 nm and the updated TEDI based on the Aura OMI and A-MODIS measurements. Based on the scatter plot, the stringent

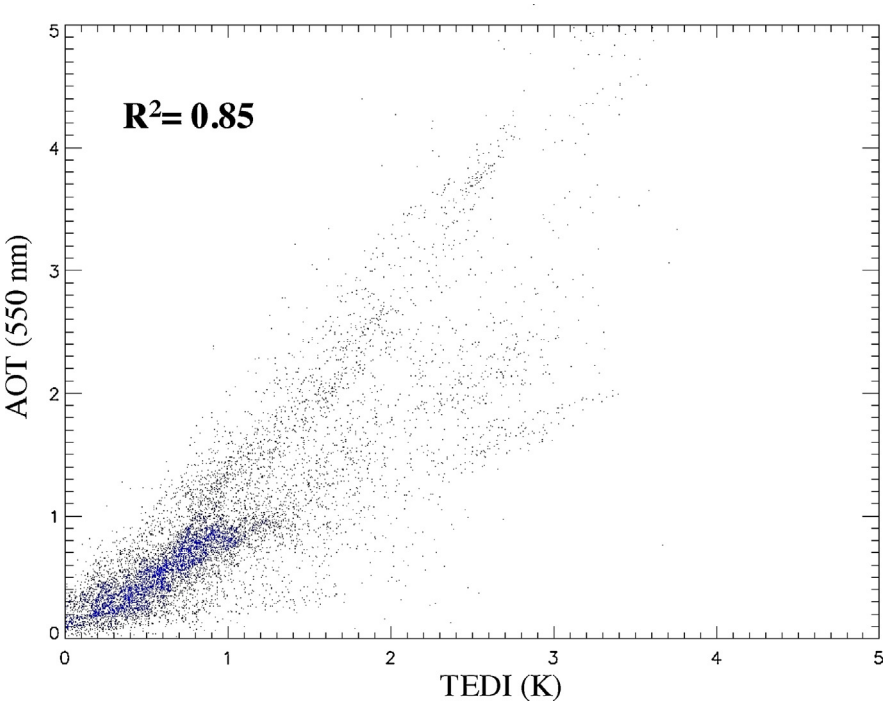

Fig. 5. Scatter plot of AOT and TEDI based on Aura OMI and A-MODIS measurements.

http://dx.doi.org/10.1016/j.heliyon.2017.e00241

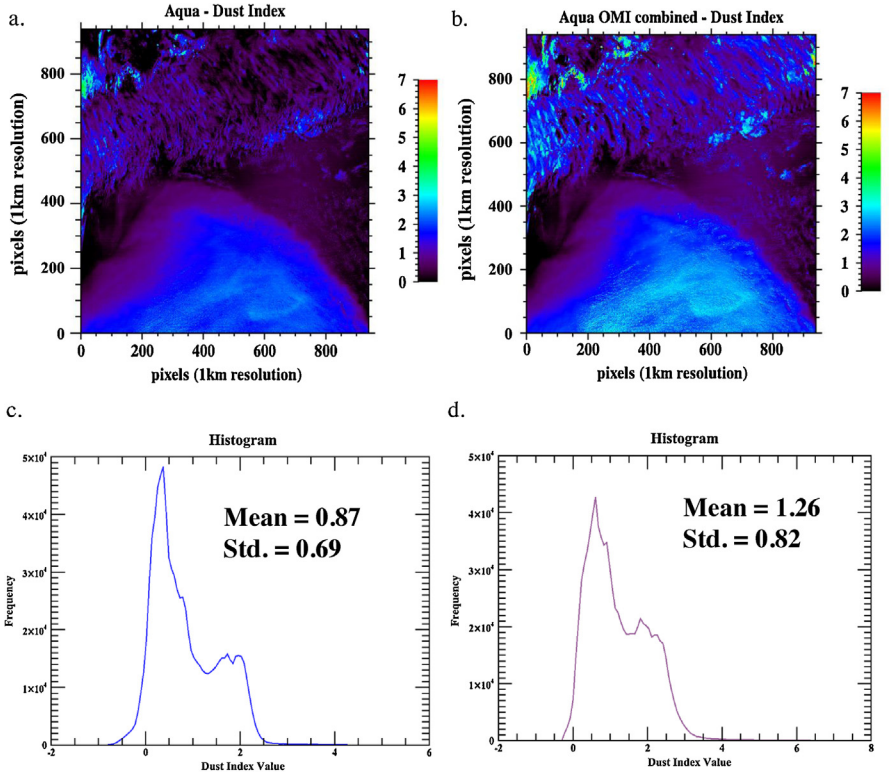

Fig. 6. Validation Scene A-MODIS (February 12, 2005): a. TEDI retrieval, b. Updated TEDI retrieval, c. Histogram AOT, d. Histogram TEDI.

dust aerosol type identified through OMI datasets has led to an increased correlation in comparison to the correlation presented by Fig. 2b. The correlation R^2 metric in fact increased to 0.85 from 0.81. This proves that the aerosol type classification indeed helped in improving the dust radiometry. The updated TEDI model is now applied to the A-MODIS validation scene as shown in Fig. 6.

Fig. 6 shows the validation scene of A-MODIS with both the original TEDI and the updated TEDI using the OMI measurements. From Fig. 6a and b, it is observed qualitative that the dust radiometry is much finer in terms of resolution based on the updated TEDI. This is further corroborated from the histogram charts shown by Fig. 6c and d. The histogram features (i.e. the various sub peaks and valleys) have far more structure in Fig. 6d in comparison to Fig. 6c. This is quantified by the increase in both the mean and standard deviations of the histogram. Thus, the updated TEDI improves the overall dust radiometry and is highly useful for monitoring Saharan dust outbreak events.

5. Conclusions

This paper focused on the dust detection scheme improving upon the previously developed technique in (Hao and Qu, 2007). The dust detection scheme was

http://dx.doi.org/10.1016/j.heliyon.2017.e00241

formed on the basis of spectral channels sensitive to dust particles. One disadvantage of the AOT was that these quantities are only retrievable from day time imagery/measurements and at much lower spatial resolution. In order to address this deficiency, the approach was extended by employing the mid and far infrared channels of MODIS. The index derived was named as Thermal Emissive Dust Index (TEDI). The TEDI significantly outperformed the AOT based detection. The key advantage was that the dust radiometry was far more enhanced and coupled with the higher spatial resolution of the derived index. The traditional AOT retrieval was based at 10 km resolution while the TEDI was derived at 1 km spatial resolution. However, further adjustments were made in the modeling by using the aerosol type information of the OMI sensor. By combining the aerosol type the dust detection scheme was further improved which gave a much improved radiometric dust index. These were novel additions to the dust detection scheme from the previous work as shown by (Hao and Qu, 2007). The result shown are very encouraging, in fact the dust index devised clearly outperformed the AOT retrieval. It was noted through the work that the AOT retrieval algorithms were not mature at a higher spatial resolution. Thus, usage of the dust detection scheme proposed here is very important for identifying dust outbreaks which significantly affects the radiative forcing of the atmosphere.

Declarations

Author contribution statement

Sriharsha Madhavan: Conceived and designed the experiments; Performed the experiments; Analyzed and interpreted the data; Contributed reagents, materials, analysis tools or data; Wrote the paper.

John Qu, Xianjun Hao: Contributed reagents, materials, analysis tools or data.

Funding statement

This research did not receive any specific grant from funding agencies in the public, commercial, or not-for-profit sectors.

Competing interest statement

The authors declare no conflict of interest.

Additional information

No additional information is available for this paper.

http://dx.doi.org/10.1016/j.heliyon.2017.e00241

Acknowledgments

The authors would like to thank Dr. Mike Summers (Department of Physics and Astronomy, GMU) and Dr. Donglian Sun (Department of Geography and Geoinformation Sciences, GMU) for their helpful comments and suggestions.

References

Ackerman, S.A., 1997. Remote sensing aerosols using satellite infrared observations. J. Geophys. Res. 102 (D14), 17069–17079.

Christensen, P.R., Bandfield, J.L., Hamilton, V.E., Howard, D.A., Lane, M.D., Piatek, J.L., Ruff, S.W., Stefanov, W.L., 2000. A thermal emission spectral library of rock-forming minerals. J. Geophys. Res. 105, 9735–9739.

Grey, W.M., North, P.J., et al., 2006. Aerosol optical depth and land surface reflectance from multi-angle AATSR measurements: global validation and inter-sensor comparisons. IEEE Trans. Geosci. Remote Sens. 44 (8), 2184–2197.

Hao, X., Qu, J.J., 2007. Saharan dust storm detection using moderate resolution imaging spectroradiometer thermal infrared bands. J. Appl. Remote Sens. 1, 1–9.

Holben, B.N., Tanre, D., Smirnov, A., Eck, T.F., Slutsker, I., Abuhassan, N., Newcomb, W.W., Schafer, J., Chatenet, B., Lavenue, F., Kaufman, Y.J., Vande Castle, J., Setzer, A., Markham, B., Clark, D., Frouin, R., Halthore, R., Karnieli, A., O'Neill, N.T., Pietras, C., Pinker, R.T., Voss, K., Zibordi, G., 2001. An emerging ground-based aerosol climatology: Aerosol Optical Depth from AERONET. J. Geophys. Res. 106, 12067–12097.

Hsu, N.C., Tsay, S., King, M.D., Herman, J.R., 2004. Aerosol Properties Over Bright-Reflecting Source Regions. IEEE Trans. Geosci. Remote Sens. 42 (3), 557–569.

Kaufman, Y.J., Tanré, D., Remer, L.A., Vermote, E.F., Chu, A., Holben, B.N., 1997. Operational remote sensing of tropospheric aerosol over land from EOS moderate resolution imaging spectroradiometer. J. Geophys. Res. 102, 17051-–17067.

Levelt, P.F., et al., 2006. The ozone monitoring instrument. IEEE Trans. Geosci. Remote Sens. 44 (5), 1093–1101.

Madhavan, S., Qu, J., Hao, X., 2016. Decadal Impact Study of Saharan Dust Transport using Multi Sensor Measurements. IJARSG 5.

Menéndez, I., Diaz-Hernandez, J.L., Mangas, J., Alonso, I., Sánchez-Soto, P.J., 2007. Airborne dust accumulation and soil development in the North-East sector of Gran Canaria (Canary Islands, Spain). J. Arid Environ. 71 (1), 57–81.

 http://dx.doi.org/10.1016/j.heliyon.2017.e00241

Mishchenko, M.I., Geogdzhayev, I.V., et al., 1999. Aerosol retrievals over the ocean by use of channels 1 and 2 AVHRR data: sensitivity analysis and preliminary results. Appl. Opt. 38 (36), 7325–7341.

Remer, L.A., Kaufman, Y.J., Tanre, D., et al., 2005. The MODIS Aerosol Algorithm Products and Validation. J. Atmos. Sci. 62, 947–973 Special Edition.

Tanré, D., Kaufman, Y.J., Herman, F., Mattoo, S., 1997. Remote sensing of aerosol properties over oceans using the MODIS/EOS spectral radiances. J. Geophys. Res. 102 (D14), 16971–16988.

Wald, A.E., 1995. Modeling thermal infrared (2-14 (m) reflectance of frost and snow. J. Geophys. Res. 99, 24241–24250.